# Wave-equation traveltime and amplitude for Kirchhoff migration

*Yu Pu*, Gang Liu, Diancheng Wang, Hui Huang, and Ping Wang, CGG*

**Summary**

Full-waveform inversion has been established as a standard tool for building high-resolution velocity models. To take full advantage of such models, the migration algorithm must be capable of handling fine-scale geo-bodies and sharp contrasts while affordably producing high-frequency migration stacks and gathers. Even though ray-based Kirchhoff migration can efficiently generate high-resolution migration stacks and gathers, the calculation of traveltimes becomes inaccurate and unstable near large velocity variations, sharp contrasts, and complex structures. Reverse-time migration (RTM), on the other hand, can accurately handle complex velocity models with fine details and sharp contrasts due to its deployment of full-wavefield propagation. However, the cost of RTM becomes prohibitive when high-frequency stacks and gathers are required. Following this idea of wave-equation-based traveltimes, we propose a wave-equation Kirchhoff (WEK) scheme that performs Kirchhoff migration using maximum-amplitude traveltimes and amplitudes from the wavefield. These traveltimes and amplitudes are computed through affordable low-frequency full-wavefield propagation. WEK not only partly inherits the benefit of full-wavefield propagation for high-resolution models, but it also maintains the affordability of ray-based Kirchhoff migration. We use synthetic and field data to evaluate this method and compare the WEK results with those from ray-based Kirchhoff migration and RTM.

**Introduction**

Full-waveform inversion (FWI) was first proposed by Lailly (1983) and Tarantola (1984) over three decades ago. With recent advancements in the FWI algorithm and compute power, FWI has been democratized for almost all industrial seismic data sets to automatically build high-resolution velocity models (Shen et al., 2018; Zhang et al., 2018, 2020; Wang et al., 2019). To take full advantage of FWI velocity models, the migration algorithm must account for fine-scale geo-bodies and sharp contrasts while also affordably producing high-frequency migration stacks and gathers.

Ray-based Kirchhoff migration is an efficient method that generates high-frequency stacks and gathers. For this reason, it is widely used in almost all stages of seismic imaging, including preprocessing, velocity model building, and final migration. However, ray-based Kirchhoff migration relies on raytracing to calculate traveltimes and the corresponding amplitudes. Raytracing requires a smoothly-varying velocity model and becomes inaccurate and unstable when a velocity model has large variations, sharp contrasts, or complex geological structures. In contrast, RTM employs full-wavefield propagation based on the wave equation and thus can accurately handle high-resolution, complex models (Zhang and Zhang, 2008). However, its cost becomes prohibitive when high-frequency products (stacks and gathers) are needed. Generating high-frequency surface offset gathers with RTM is even more prohibitive (Yang et al., 2015).

For Kirchhoff migration to utilize high-resolution, complex velocity models, several authors have proposed strategies to replace ray-based traveltime calculations with wave-equation based methods. Nichols (1996) proposes a maximum energy traveltime calculation from the Helmholtz equations at a few frequencies within the seismic frequency band. Ehinger et al. (1996) and Etgen (2012) propose Kirchhoff migration using Green's function computed with wavefield extrapolation techniques based on a finite-difference implementation of the wave equation. Andrade et al. (2015) show a method to calculate maximum amplitude traveltimes with the Chebyshev polynomial recursion. With the advancement in computer capabilities, Jin and Etgen (2020) directly generate maximum-amplitude traveltimes using finite-difference solutions to the full wave equation. Their solution is limited within a low-frequency band to reduce cost, but still achieves considerable improvement in stack coherence and gather flatness.

In our wave-equation Kirchhoff (WEK) scheme, we similarly simulate full-wavefield propagation at low frequencies (e.g., 10-20 Hz), but we derive both the traveltimes and amplitudes to be used in Kirchhoff migration from the maximum-amplitude arrival. We apply WEK on one 2.5D synthetic data set and two 3D field data sets to demonstrate its benefits over ray-based Kirchhoff migration.

**Method**

In our implementation of the Kirchhoff migration, we follow the general formulation proposed by Bleistein et al. (1998):

$$R(\boldsymbol{x}) \sim \frac{1}{8\pi^3} \int w(\boldsymbol{x}, \boldsymbol{\xi}) e^{i\omega(\tau_s+\tau_r)} u_s(\boldsymbol{x_r}, \boldsymbol{x_s}, \omega) i\omega d\omega d\boldsymbol{\xi}, \quad (1)$$

where the weighting function is written as

$$w(\boldsymbol{x}, \boldsymbol{\xi}) = \frac{|h(\boldsymbol{x}, \boldsymbol{\xi})|}{A(\boldsymbol{x}, \boldsymbol{x_s}) A(\boldsymbol{x_r}, \boldsymbol{x}) |\nabla(\tau_s + \tau_r)|^2}$$

with the Beylkin determinant

$$h(\boldsymbol{x}, \boldsymbol{\xi}) = det \begin{vmatrix} \nabla(\tau_s + \tau_r) \\ \frac{\partial}{\partial \xi_1} \nabla(\tau_s + \tau_r) \\ \frac{\partial}{\partial \xi_2} \nabla(\tau_s + \tau_r) \end{vmatrix}.$$

Coordinates $\boldsymbol{x_s}(\boldsymbol{\xi})$, $\boldsymbol{x_r}(\boldsymbol{\xi})$ and $\boldsymbol{x}$ are source, receiver, and image points, respectively, where $\boldsymbol{\xi} = (\xi_1, \xi_2)$ parameterizes the acquisition surface over the shots/receivers range. $\tau_s/\tau_r$ is the traveltime between source/receiver and image point, which can be found by solving the eikonal equation (Aki and Richards, 1980; Gray and May, 1994):

$$\nabla\tau \cdot \nabla\tau - \frac{1}{c^2} = 0, \quad (2)$$

where $c$ is the medium velocity. $A(\boldsymbol{x}, \boldsymbol{y})$ is the amplitude of Green's function between $\boldsymbol{x}$ and $\boldsymbol{y}$, which can be calculated by solving the associated transport equation:

$$\nabla^2\tau + \frac{2}{A}\nabla A \cdot \nabla\tau = 0. \quad (3)$$



10.1190/segam2021-3583642.1

Equations 2 and 3 adopt the high-frequency asymptotic assumption, and therefore are only valid when the medium velocity varies slowly. For Equation 1 to handle fine-scale geo-bodies and strong velocity contrasts (e.g., velocity models from high-frequency FWI, carbonate layers, and salt boundaries), we propose replacing the traveltimes (Equation 2) and amplitudes (Equation 3) by those derived from the wavefield $u$ computed by full-wavefield propagation:

$$\left(\frac{1}{c^2}\frac{\partial}{\partial t^2} - \nabla^2\right) u(\boldsymbol{x}, \boldsymbol{x_s}, t) = \delta(\boldsymbol{x}, \boldsymbol{x_s}) f(t), \qquad (4)$$

where $\delta(\boldsymbol{x}, \boldsymbol{x_s})$ describes a point source located at $\boldsymbol{x_s}$ and $f(t)$ is the source wavelet. We call this approach wave-equation Kirchhoff (WEK), and it consists of three main steps: 1) place a point source and forward propagate the wavefield for each surface location; 2) derive a traveltime and amplitude of the maximum-amplitude arrival at each subsurface location; and 3) apply the derived traveltime and amplitude to Kirchhoff migration as described in Equation 1.

### 2.5D synthetic data example

Our first example is a 2.5D synthetic data test using the Marmousi2 model. In this test, we used 3D full-wavefield propagation to create 45 Hz synthetic data from the velocity model (Figure 1a) and its corresponding Gardner density at 250 m shot spacing and 25 m receiver spacing. The maximum offset is 8 km in the inline direction and 250 m in the crossline direction. Calculating accurate traveltimes is key to the success of this migration because the Marmousi2 model has complicated structures and sharp velocity contrasts in the central area. However, accurate traveltimes are difficult to calculate when using conventional ray-based Kirchhoff migration, especially when imaging the deep events in the center of the test area. In this case, ray-based Kirchhoff migration results in a smeared image in the middle of Figure 1c, as indicated by the red arrows. WEK, in contrast, computes more accurate traveltimes using full-wavefield propagation, and subsequently reveals more details in the central part, as indicted by the green arrows in Figure 1d. These events look more coherent in the WEK stack and are well aligned with the reflectivity in Figure 1b, which is the zero-angle reflectivity calculated from velocity and the corresponding Gardner density. The deep central events are also apparent in the WEK gathers in Figure 1f, while they are absent in the ray-based Kirchhoff gathers in Figure 1e. The above synthetic test demonstrates that WEK surpasses conventional ray-based Kirchhoff migration for this complicated Marmousi2 model.

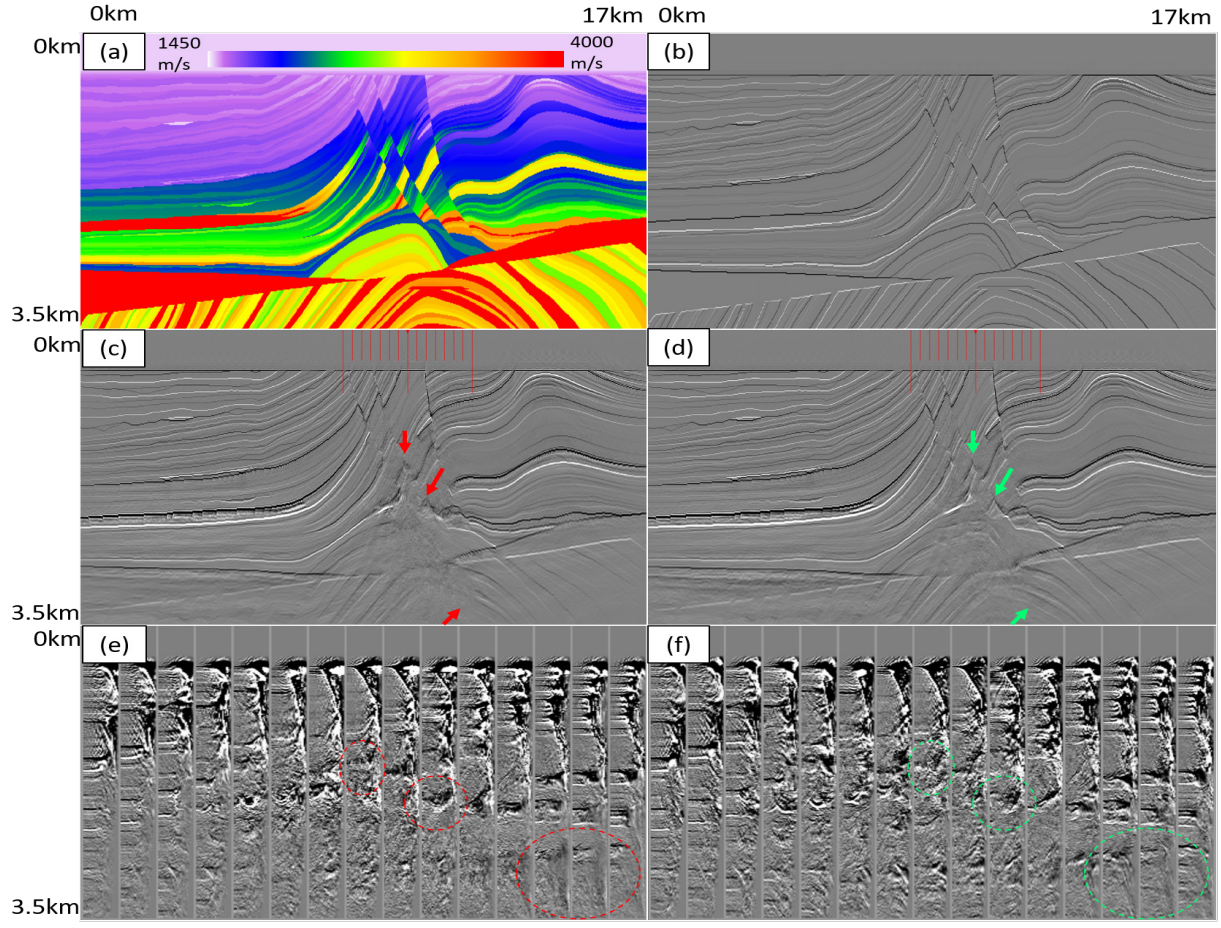


**Figure 1**: Synthetic data example: (a) Marmousi2 velocity model, (b) zero-angle reflectivity, (c) ray-based Kirchhoff stack, (d) WEK stack, (e) ray-based Kirchhoff gathers, and (f) WEK gathers.

DOI:10.1190/segam2021-3583642.1

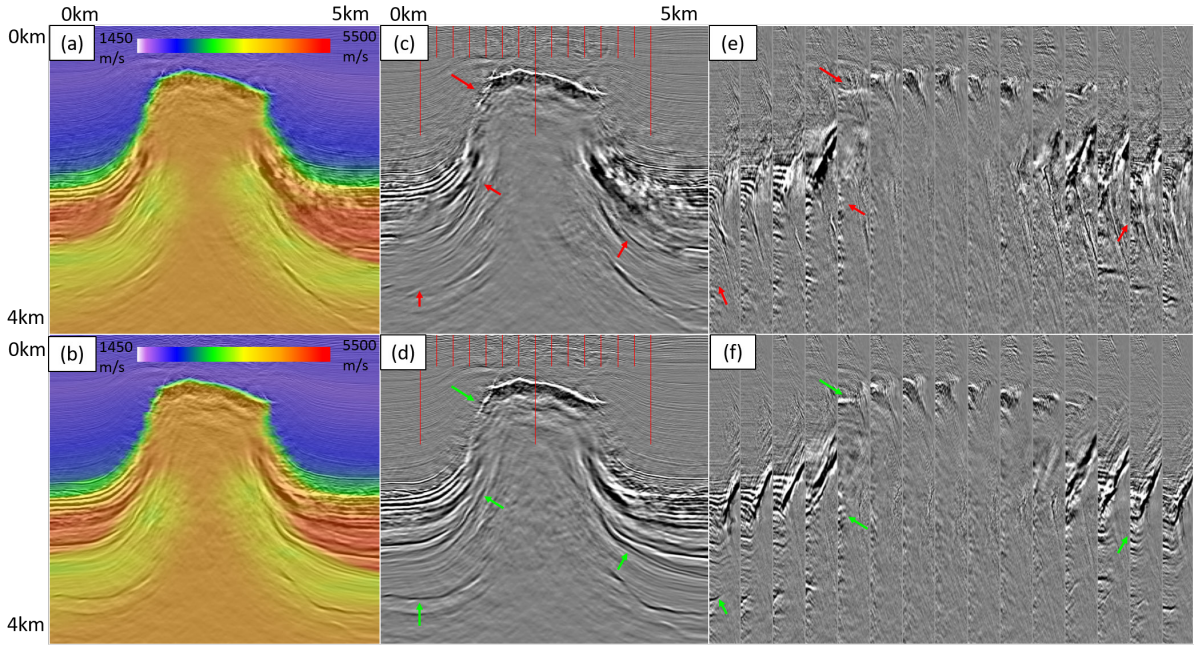


**Figure 2**: Salt diapir in the Central North Sea: (a) velocity model and ray-based Kirchhoff stack, (b) velocity model and WEK stack, (c) ray-based Kirchhoff stack, (d) WEK stack, (e) ray-based Kirchhoff gathers, and (f) WEK gathers. CGG Multi-Client Cornerstone data.

### 3D field data examples

We now apply WEK on two field data sets to evaluate its effectiveness in imaging complex geology for real surveys.

The first field data example is from a narrow-azimuth streamer survey in the Central North Sea. Figure 2 shows image comparisons around a salt diapir, with the inline section of the velocity model shown in Figures 2a and 2b. Events indicated by the red arrows in Figure 2c are not clearly imaged by the conventional ray-based Kirchhoff migration. This implies that raytracing fails to give the correct traveltimes around the diapir, where the velocity varies quickly and the geology is not simple. On the other hand, Figure 2d demonstrates how WEK brings an apparent uplift in stack coherence (green arrows), especially for events near the flanks of the salt. From the gathers in Figure 2f, we also observe that most of the WEK improvement comes from the near offsets. These coherent near-offset events are not present in the ray-based Kirchhoff migration gather (Figure 2e).

The second field data example uses a towed-streamer survey in the Walker Ridge area of the US Gulf of Mexico. Figure 3a displays an inline section of the velocity model near Walker Ridge, showing complicated salt structures and slow-velocity regions. Such geological complexity and velocity anomalies pose a significant challenge for traveltime computation in ray-based Kirchhoff migration. Red arrows in Figure 3c point to subsalt events with poor coherence in the ray-based Kirchhoff stack. In contrast, WEK shows better coherence at these locations, as indicated by the green arrows in Figure 3d. Uplift from WEK is also evident when comparing the ray-based Kirchhoff migration gathers (Figure 3e) with the WEK gathers (Figure 3f). We have included a 25 Hz RTM image in Figure 3b as a reference to compare the migration stacks. In terms of kinematics and coherence, the WEK image shows higher agreement with the RTM image than the ray-based Kirchhoff image does. The RTM image still looks superior because it naturally takes multi-pathing into account, while WEK only considers one single maximum-amplitude arrival. However, it will be very computationally expensive for RTM to create high-frequency common offset gathers like those in Figure 3f.

### Conclusions and discussion

We have presented Kirchhoff migration results (stack and gathers) using both traveltimes and amplitudes derived from the wavefield computed by full-wavefield propagation. Synthetic and field data examples show that WEK can successfully account for fine-scale geo-bodies and sharp velocity contrasts and thus improve image quality in these settings when compared with ray-based Kirchhoff migration. WEK can be a useful additional tool for validating and utilizing high-frequency FWI velocity models.

Despite picking traveltimes and amplitudes on a low-frequency wavefield (e.g., 10-20 Hz) for affordable compute cost, we found that the picking accuracy is much higher than the theoretical limit of half wavelengths. In addition, once the time is determined, the full-bandwidth time-domain seismic data can be mapped to the depth domain to produce high-resolution images.

Nichols (1996) and Nguyen and McMechan (2013) demonstrate that a single maximum-amplitude arrival should produce comparable images to using full arrivals in most cases. However, when the velocity model contains

many details with large contrasts (e.g., rugose top-of-salt), the wavefield becomes very complex with multiple arrivals. Multi-arrival picking may help to some extent but is very difficult to do correctly. Therefore, RTM may still be the best choice in such cases. On the other hand, when the velocity model is simple, the benefit of WEK over ray-based Kirchhoff diminishes quickly. In short, we expect the quality benefit of WEK will only be evident for some specific geologic settings, such as salt domes.

**Acknowledgments**

We thank CGG for permission to publish this work and CGG Multi-Client for permission to use the Walker Ridge Gulf of Mexico and Cornerstone Central North Sea data examples.

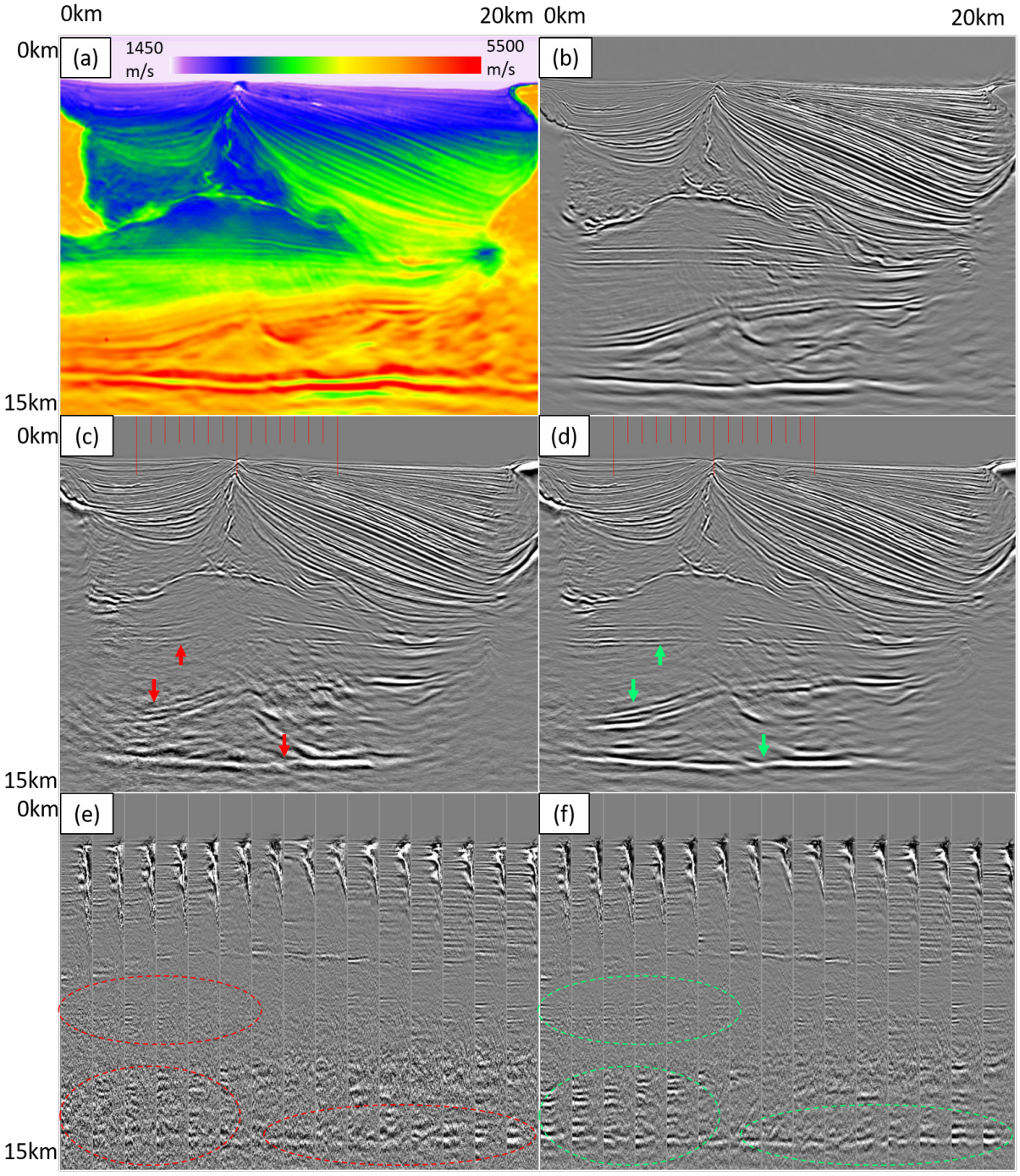


**Figure 3**: Walker Ridge area in the US Gulf of Mexico: (a) velocity model, (b) RTM stack, (c) ray-based Kirchhoff stack, (d) WEK stack, (e) ray-based Kirchhoff gathers, and (f) WEK gathers. CGG Multi-Client Walker Ridge data.

## REFERENCES


Aki, K., and P. G. Richards, 1980, Quantitative seismology: Theory and methods: W. H. Freeman and Co.

Andrade, P. N., R. C. Pestana, and A. W. G. dos Santos, 2015, Kirchhoff depth migration using maximum amplitude traveltimes computed by the Chebyshev polynomial recursion: 14th International Congress of the Brazilian Geophysical Society and EXPOGEF, Expanded Abstracts, 1109–1113, doi: https://doi.org/10.1190/sbgf2015-221.

Bleistein, N., J. K. Cohen, and J. W. Stockwell, 1998, Mathematics of multidimensional seismic imaging, migration, and inversion: Springer.

Ehinger, A., P. Lailly, and K. J. Marfurt, 1996, Green's function implementation of common-offset wave equation migration: Geophysics, **61**, 6, 1813–1821, doi: https://doi.org/10.1190/1.1444097.

Etgen, J. T., 2012, 3D wave equation Kirchhoff migration: 82nd Annual International Meeting, SEG, Expanded Abstracts, doi: https://doi.org/10.1190/segam2012-0755.1.

Gray, S. H., and W. P. May, 1994, Kirchhoff migration using eikonal equation traveltimes: Geophysics, **59**, 5, 810–817, doi: https://doi.org/10.1190/1.1443639.

Jin, H., and J. Etgen, 2020, Evaluating Kirchhoff migration using wave-equation generated maximum amplitude traveltimes: 90th Annual International Meeting, SEG, Expanded Abstracts, 2968–2972, doi: https://doi.org/10.1190/segam2020-3425618.1.

Lailly, P., 1983, The seismic inverse problem as a sequence of before stack migrations, *in* J. B. Bednar, R. Redner, E. Robinson, and A. Weglein, eds., Conference on inverse scattering: Theory and application: SIAM, 206–220.

Nguyen, B. D., and G. A. McMechan, 2013, Excitation amplitude imaging condition for prestack reverse-time migration: Geophysics, **78**, no. 1, S37–S46, doi: https://doi.org/10.1190/geo2012-0079.1.

Nichols, D. E., 1996, Maximum energy traveltimes calculated in the seismic frequency band: Geophysics, **61**, no. 1, 253–263, doi: https://doi.org/10.1190/1.1443946.

Shen, X., L. Jiang, J. Dellinger, A. Brenders, C. Kumar, M. James, J. Etgen, D. Meaux, R. Walters, and N. Abdullayev, 2018, High resolution full waveform inversion for structural imaging in exploration: 88th Annual International Meeting, SEG, Expanded Abstracts, 1098–1102, doi: https://doi.org/10.1190/segam2018-2997202.1.

Tarantola, A., 1984, Inversion of seismic reflection data in the acoustic approximation: Geophysics, **49**, no. 8, 1259–1266, doi: https://doi.org/10.1190/1.1441754.

Wang, P., Z. Zhang, J. Mei, F. Lin, and R. Huang, 2019, Full-waveform inversion for salt: A coming of age: The Leading Edge, **38**, 204–213, doi: https://doi.org/10.1190/tle38030204.1.

Yang, Z., S. Huang, and R. Yan, 2015, Improved subsalt tomography using RTM surface offset gathers: 85th Annual International Meeting, SEG, Expanded Abstracts, 5254–5258, doi: https://doi.org/10.1190/segam2015-5848366.1.

Zhang, H., and Y. Zhang, 2008, Reverse time migration in 3D heterogeneous TTI media: 78th Annual International Meeting, SEG, Expanded Abstracts, 2196–2200, doi: https://doi.org/10.1190/1.3059322.

Zhang, Z., J. Mei, F. Lin, R. Huang, and P. Wang, 2018, Correcting for salt misinterpretation with full-waveform inversion: 88th Annual International Meeting, SEG, Expanded Abstracts, 1143–1147, doi: https://doi.org/10.1190/segam2018-2997711.1.

Zhang, Z., Z. Wu, Z. Wei, J. Mei, R. Huang, and P. Wang, 2020, FWI Imaging: Full-wavefield imaging through full-waveform inversion: 90th Annual International Meeting, SEG, Expanded Abstracts, 656–660, doi: https://doi.org/10.1190/segam2020-3427858.1.